nature materials

LETTERS

PUBLISHED ONLINE: 20 APRIL 2014 | DOI: 10.1038/NMAT3927

Optical Fano resonance of an individual semiconductor nanostructure

Pengyu Fan[1]*, Zongfu Yu[2], Shanhui Fan[2] and Mark L. Brongersma[1]*

Fano resonances with a characteristic asymmetric line shape can be observed in light scattering, transmission and reflection spectra of resonant optical systems[1]. They result from interference between direct and indirect, resonance-assisted pathways. In the nanophotonics field, Fano effects have been observed in a wide variety of systems, including metallic nanoparticle assemblies[2], metamaterials[2,3] and photonic crystals[4,5]. Their unique properties find extensive use in applications, including optical filtering, polarization selectors, sensing, lasers, modulators and nonlinear optics[6–11]. We report on the observation of a Fano resonance in a single semiconductor nanostructure, opening up opportunities for their use in active photonic devices. We also show that Fano-resonant semiconductor nanostructures afford the intriguing opportunity to simultaneously measure the far-field scattering response and the near-field energy storage by extracting photogenerated charge. Together they can provide a complete experimental characterization of this type of resonance.

The advances in the field of plasmonics have made it possible to engineer the optical coupling in metallic nanoparticle assemblies to produce strong Fano resonances[12–14]. This is accomplished by spectrally placing a broad and a narrow scattering resonance of a system on top of each other. The coherent interference between the two scattering pathways produces a characteristic asymmetric Fano line shape[15]. Fano resonances obtained from subwavelength scatterers are of particular interest as an analysis of the line shape can reveal many insights into the coherent, near-field optical interactions in such nanoscale systems that typically remain hidden in a far-field light scattering experiment[16]. To obtain a complete picture behind the origin and nature of a Fano resonance, it is required to quantify the frequency-dependent energy storage that occurs in the resonant scattering pathway. The stored energy in metallic nanostructures is dissipated as heat and can be accessed only by challenging near-field optical techniques[17] or nonlinear generation[18]. In this work, we show that Fano resonances can be obtained in single semiconductor nanostructures. Moreover, we demonstrate that these structures facilitate a convenient simultaneous measurement of the far-field scattering and near-field energy storage to enable a complete experimental characterization of these nanophotonic resonators.

Semiconductor nanowires support a series of optical resonances[19,20] that give rise to strong light scattering and absorption. These properties have been applied for structural colour[21], light localization[22], compact and efficient photodetection[23], thermal emitters[24], solar cells[25] and other new optoelectronic devices[26]. The resonant wavelengths in the nanowires can be tuned by changing their size[20], cross-sectional shape[25] and environment[21].

Figure 1a illustrates how a one-dimensional semiconductor nanostructure affords simultaneous measurement of its scattering and absorption resonances. When the structure is illuminated from the top, the scattered light can be analysed in bright- and dark-field configurations in an optical microscope. With electrical contacts at the two terminations, the structure is turned into a metal–semiconductor–metal (MSM) photodetector whose photocurrent provides a direct measure of the light absorption in the semiconductor region. The light absorption in the wire with a volume V at an illumination angular frequency ω is in turn linked to the optical energy storage in the nanowire as: $(A = \int \omega \cdot \mathrm{Im}(\varepsilon) \cdot |E|^2 \cdot \mathrm{d}V)$. Here, $\mathrm{Im}(\varepsilon)$ is the imaginary part of the dielectric constant that determines the intrinsic light absorption properties of the semiconductor and E is the electric field of the light. Figure 1b shows a scanning electron microscope (SEM) image of a 220-nm-wide and 50-nm-high polycrystalline silicon (Si) nanostripe photodetector generated by photolithographic means (see Methods). We analyse the Fano resonance produced by this device.

The observation of a Fano resonance in a subwavelength semiconductor nanostructure has thus far been elusive. This can be explained by the fact that most light scattering studies have focused on spherical and cylindrical nanorod geometries for which the observation of such resonances is challenging[2]. We start by providing intuition why reshaping a semiconducting cylinder into a judiciously shaped stripe can result in the observation of a clear Fano resonance in the total scattering efficiency Q_{TS}. This quantity is defined as the ratio of the total scattering cross-section and the geometrical cross-section, taken as the width of the stripe. We will then also show that this enables experimental observation of a Fano resonance in a differential, backscattering efficiency Q_{BS} measured in our experiments[19]. From Mie theory, it is known that the spectrum of the total scattering efficiency of a cylinder shows a series of resonances related to the excitation of orthogonal modes with different angular momenta, termed the dipolar, quadrupolar and so on, channels[19]. Owing to the mode-orthogonality, the spectra of the total scattering efficiency do not show any effects of inter-channel interference between the distinct angular-momentum scattering channels. As a result, the spectrum of Q_{TS} can be obtained by linearly summing the contributions from all of the relevant scattering channels. For completeness, it is worth mentioning that inter-channel interference effects can be observed in the differential back- and forward-scattering spectra[2].

For our work, it is important to realize that each angular momentum channel supports a resonant and non-resonant pathway and a Fano resonance can thus, at least in principle, occur in the spectrum of Q_{TS} as a result of intra-channel interference.

[1]Geballe Laboratory for Advanced Materials, Stanford University, Stanford, California 94305, USA, [2]Department of Electrical Engineering, Stanford University, Stanford, California 94305, USA. *e-mail: pengyu.fan@gmail.com; brongersma@stanford.edu

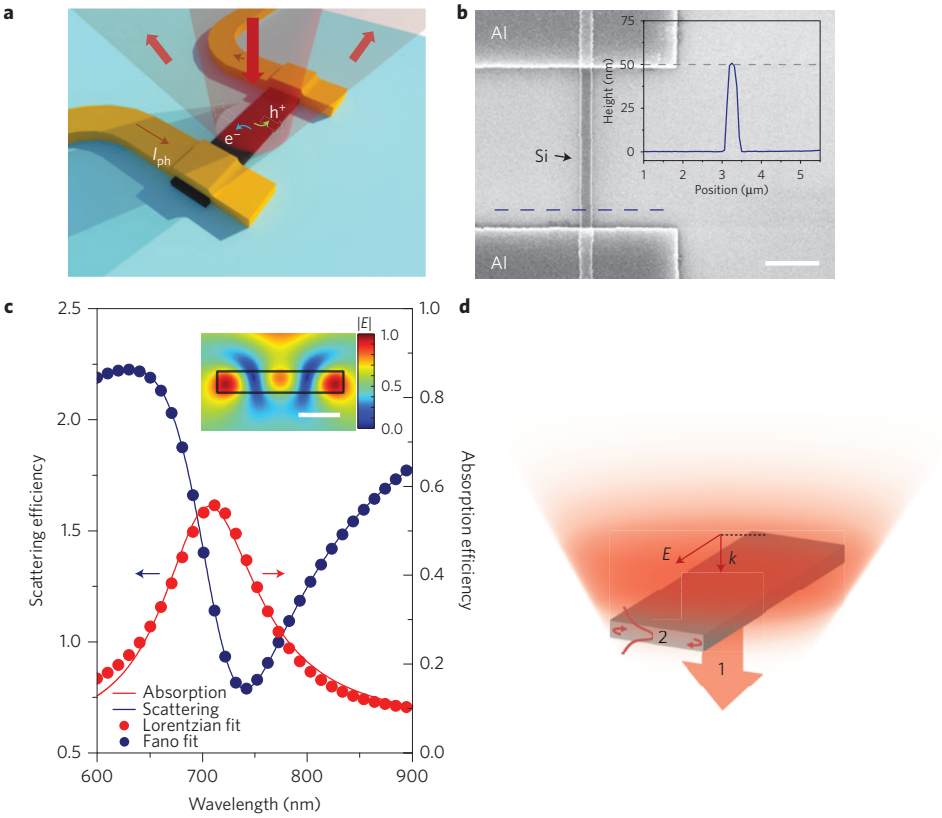

Figure 1 | Near and far-field characterization of Fano resonances in a high-index semiconductor nanostructure. a, Schematic illustrating how a semiconductor nanostripe enables measurement of the far-field scattering and near-field energy storage using a photocurrent measurement. **b**, SEM image of a fabricated Si nanostripe photodetector. Scale bar, 1 μm. Inset shows a line-cut of an atomic force microscope measurement along the cross-section of the stripe (indicated by the blue dashed line) showing that the thickness of the Si nanostripe is 50 nm. **c**, Simulated total scattering (blue) and absorption efficiency (red) spectra of a 300-nm-wide and 50-nm-thick semiconductor stripe (represented by the black rectangle in the inset). The dots represent results acquired from numerical simulations and the solid lines represent a Lorentzian fit to the absorption (red) spectrum and a Fano fit for the scattering spectrum (blue). Inset shows the distribution in the electric field intensity at the resonant frequency of 422 THz ($\lambda = 710$ nm). The field intensity is normalized to its maximum value. Scale bar, 100 nm. **d**, Schematic illustrating our intuitive understanding of the Fano resonance supported by a subwavelength semiconducting stripe showing the interference between a non-resonant pathway (labelled 1) in which light is directly reflected by/transmitted through the stripe and a resonant pathway (labelled 2) where the light couples to a standing-wave resonance of the stripe.

This explains the Fano resonances observed from subwavelength stripes. Fano resonances due to intra-channel interference within a single angular momentum channel have previously been observed for metallic cylinders[27]. For subwavelength dielectric cylinders, the resonant pathway dominates the non-resonant one and the spectra of Q_{TS} and the absorption efficiency Q_A feature a series of symmetric peaks[20] (Supplementary Figs 1 and 2). For large and wide stripes additional interference pathways become accessible that can give rise to Fano resonances. This can be seen from a multiple-multipole expansion, where the electromagnetic field is decomposed into multipoles placed at appropriate locations inside the object. The fields with different angular momentums that originate from different locations in such stripes are no longer orthogonal and can interfere.

Figure 1c shows how a Fano resonance can be obtained in the visible spectral range for a semiconductor nanostripe ($\varepsilon_s = 16.0 + i$) featuring a low aspect ratio (50 nm thick and 300 nm wide). Whereas the spectrum of the absorption efficiency Q_A shows a symmetric peak, the Q_{TS} spectrum shows a Fano line shape.

An analysis of the field distribution near the stripe on resonance ($\lambda = 710$ nm) affords valuable insights into the nature of the stripe resonance (see Fig. 1c inset). The effectiveness of such an analysis was previously illustrated for wavelength-scale metallic stripes[28]. The field distribution shows a clear standing wave pattern with three anti-nodes in the electric field intensity along the width of the stripe. In the Supplementary Information it is argued that this pattern results from the constructive interference of counter-propagating waves guided by the Si stripe that reflect from the stripe terminations (Supplementary Fig. 2). The anti-node spacing is governed by the effective mode index of the fundamental, transverse electric (with electric field normal to the wave vector) waveguide mode supported by a 50-nm-thick semiconductor slab. This resonance gives rise to the strong absorption peak seen in Fig. 1c.

A fraction of the resonantly stored energy in the stripe is rescattered. This resonantly scattered light will interfere with light that follows a non-resonant pathway in which it is simply being reflected or transmitted by the stripe (Fig. 1d). As compared with the non-resonant pathway, the resonant pathway features a rapidly varying amplitude and phase near the resonance frequency. As such, the interference of the two pathways can give rise to a Fano line shape.

Fano line shapes are most pronounced when the two scattering pathways are of similar magnitudes. The stripe geometry allows for a convenient geometric tuning of the strengths of the resonant and non-resonant channels; in moving from a beam with a square cross-section to a low-aspect-ratio stripe of the same height, the lateral dimension and thus the magnitude of the non-resonant channel can be increased to match the strength of the resonant channel. The evolution of Q_{TS} with increasing stripe width shows a symmetric resonance for small widths and Fano-like resonances

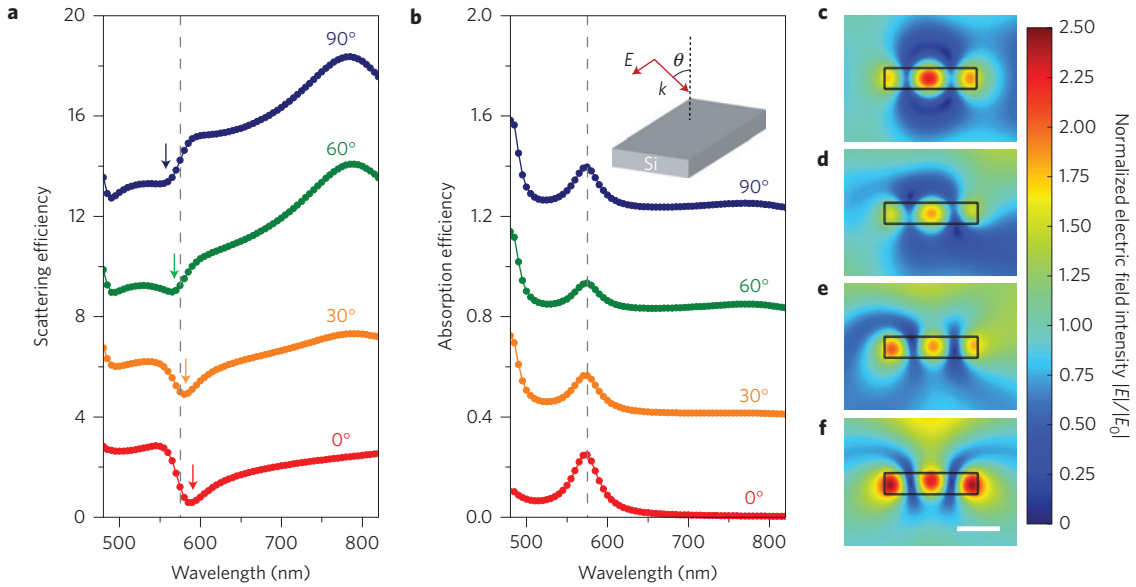

Figure 2 | Theoretical study of the Fano resonance observed from a Si nanostripe under different illumination conditions. a,**b**, Total scattering efficiency spectra (**a**) and absorption efficiency spectra (**b**) of a 220-nm-wide and 50-nm-thick Si nanostripe under different illumination angles θ as defined in the inset to **b** and with the electric field polarized along the stripe length. The vertical dashed grey lines represent the absorption resonance peak position located at 580 nm. The arrows on the scattering spectra highlight the variation of the position of the dip in scattering spectra at different incident angles. **c**–**f**, The distributions in the electric field intensity near the stripe (black rectangle) illuminated at a wavelength of 580 nm for different incident angles: 90° (**c**), 60° (**d**), 30° (**e**) and 0° (**f**; normal incidence). The electric field intensity is normalized to the incident field intensity $|E_0|$ where 1 corresponds to the incident field intensity. Scale bar, 100 nm.

for wider widths (Supplementary Fig. 2). The relative importance of the resonant and non-resonant pathways can be quantified by analysing the expression for the total scattering cross-section that was first proposed by Fano[1]:

$$\sigma_{TS}(\omega) \propto \frac{\left(q\frac{\Gamma}{2}+\omega-\omega_0\right)^2}{\left(\frac{\Gamma}{2}\right)^2+(\omega-\omega_0)^2} \quad (1)$$

Here, ω_0 is the resonant frequency; Γ is the full-width at half-maximum of the resonance. The asymmetry parameter q describes the ratio of resonant scattering amplitude to the non-resonant background scattering amplitude. The phenomenological formula predicts that, in the case of $q \gg 1$ (resonant scattering amplitude dominates), the scattering will assume a conventional symmetric Lorentzian line shape. This is the case for high-index, subwavelength-diameter cylinders (Supplementary Figs 1 and 2). When $q \sim 1$ (non-resonant and resonant scattering amplitudes are comparable), the effect of interference is more prominent and the scattering will show a Fano line shape. A fit of equation (1) to the scattering spectrum of the stripe is shown in Fig. 1c and yields: $q = 0.44$. A more detailed understanding of the interplay between resonant and non-resonant scattering pathways can be achieved using temporal coupled-mode theory[29].

Next, properties of the Fano resonance in Si nanostripes with realistic material dispersion are studied by experiment and simulation. From simulations, it was determined that a Si stripe with a width of 220 nm and a thickness of 50 nm supports a resonance at a wavelength of 580 nm. Here, the width of the stripe accommodates one-and-a-half wavelengths (1.5λ) of the fundamental transverse electric mode supported a 50-nm-thick Si slab and the electric field distribution shows three strong anti-nodes along the width of the stripe (Fig. 2c–f). The simulated Q_{TS} spectrum of the Si stripe shows a Fano line shape with a dip that appears close to, but not exactly at its absorption resonance. As the illumination angle of incidence changes from 0° (normal incidence) to 90°, the scattering spectrum significantly changes. The dip in the scattering spectrum gradually blueshifts from one side to the other side of the resonance at 580 nm (Fig. 2a). The shape of the asymmetric swing also changes with incident angle. This variation in the scattering line shape with illumination direction is a direct consequence of the changes in the interference between resonant and non-resonant scattering pathways. In contrast, the spectral line shape and peak position of the absorption spectra of the Si stripe under different incident angles remain nearly constant. This is expected as the absorption spectrum is governed by the near-field energy storage nature of the resonant mode, rather than being dictated by far-field interference. Calculated electric field distributions at the resonant wavelength under different angles (Fig. 2c–f) all show three anti-nodes along the width of the stripe, indicating essentially the same resonant mode is excited at all incident angles. These calculations further showcase that the scattering and absorption response of a Fano resonance could significantly deviate from each other and each contains different information.

We experimentally analysed the dependence of the Fano resonance on the stripe width and on incidence angle using the dark-field and bright-field illumination schemes shown in Fig. 3a,b. In one case the stripes were top-illuminated at near-normal incidence (Fig. 3a) and in the other a standard dark-field illumination configuration was used to illuminate the stripes under grazing incidence (Fig. 3b). Light was collected over a broad angular range in the backscattering direction. Figure 3c–e show SEM images of fabricated Si nanostripes of different widths (180, 200, 220 nm). On the basis of the nature of the resonance, it is expected that the resonance wavelength will redshift for increasing stripe width. The scattering spectra for top-illumination are shown in Fig. 3f, and each spectrum shows a distinct peak and valley that redshift with increasing stripe width. These spectral features provide clear evidence of a Fano resonance. Under dark-field illumination, the scattering spectra of all three stripes are modified in a similar fashion: the peaks/valleys blueshift to a shorter wavelength, a trend previously shown as a direct consequence of change in far-field interference between different scattering channels. These observed

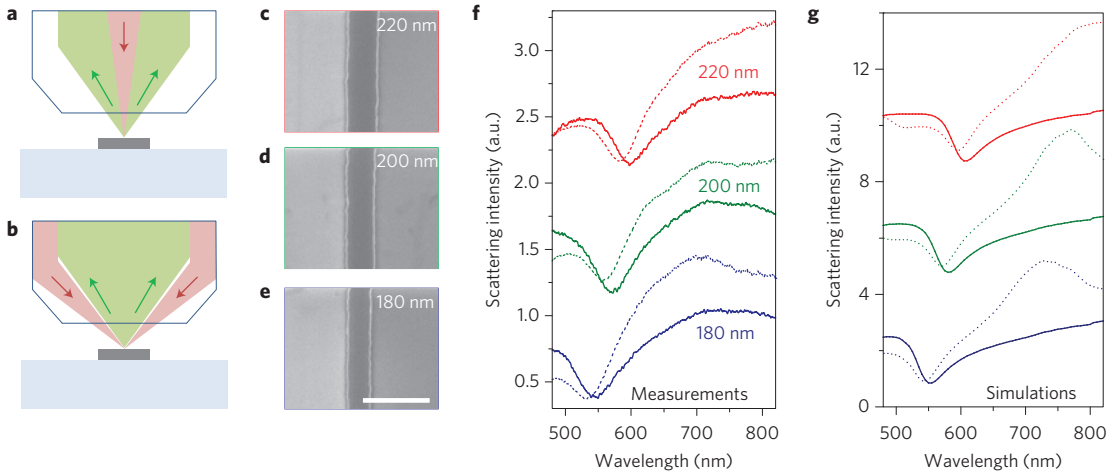

Figure 3 | Measurement and simulation of the scattering spectra of Si nanostripes. a,**b**, Illumination configurations for the scattering measurements in which white light (red arrows) is directed onto a Si stripe (grey) under near-normal incidence (**a**) or grazing incidence ($\theta \approx 50°$; **b**) through a dark-field objective. The scattered light (green arrows) is collected through the same objective in the backscattering direction. **c**–**e**, SEM images of 50-nm-thick Si nanostripes with widths of 220 nm (**c**), 200 nm (**d**) and 180 nm (**e**). Scale bar, 500 nm. **f**, Measured scattering spectra for the three different Si nanostripes (red, 220 nm; green, 200 nm; blue, 180 nm) under normal incidence (solid) and grazing incidence (dashed). **g**, Simulated scattering spectra for the same Si nanostripe sizes and the same illumination conditions (solid, normal; dashed, grazing) as in the measurements.

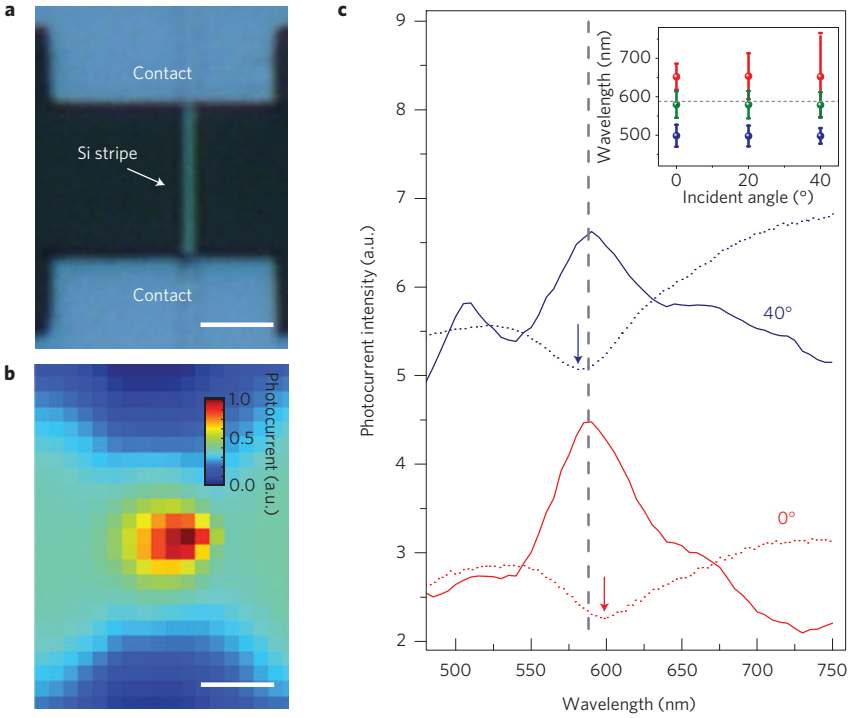

Figure 4 | Measured absorption spectra from a Si nanostripe for different illumination conditions. a, Optical image of a fabricated Si nanostripe photodetector with a 220-nm-wide and 50-nm-thick Si stripe connected to two electrical contact pads. Scale bar, 1.5 μm. **b**, A scanning photocurrent map of the device region shown in **a**, where the colour represents the magnitude of the photocurrent. **c**, Solid curves represent the measured photocurrent from the nanostripe detector as a function of the incident wavelength under normal (red) and 40° incidence (blue). The measured scattering spectra from the same structure under small (red) and large (blue) incident angles are shown for reference (dotted curves) with arrows marking the positions of the scattering minima near resonance. The vertical dashed grey line highlights the peak position of the 1.5λ absorption resonance at 580 nm. The inset shows the experimentally determined peak locations of the 1.5λ resonance and the adjacent two resonances as a function of incident angle. The data points represent the peak wavelength and the bars represent the full-width at half-maximum of the peaks.

scattering properties of Si stripes under different incident angles agree with full-field electromagnetic simulations shown in Fig. 3g, further confirming the presence of a Fano resonance.

To analyse the spectral dependence of the near-field energy storage in the stripes, they were converted into MSM photodetector structures. Figure 4a shows how the 220-nm-wide Si nanostripe was hooked up with two metallic electrodes that facilitate extraction of photocurrent from an illuminated stripe. The photocurrent is proportional to the light absorption inside the Si stripe. Figure 4b shows a photocurrent map from the stripe, obtained by raster-scanning a focused illumination spot over the stripe and measuring the photocurrent at each position. The highest photocurrent is

obtained when the illumination spot is located directly over the stripe.

Figure 4c shows the photocurrent spectra of the Si nanostripe detector under normal and grazing incidence. In both cases, a symmetric absorption peak can be identified at the same resonant wavelength of 580 nm, corresponding to the excitation of the 1.5 λ resonant mode supported by the Si stripe. The changes in the scattering spectra and fixed location of the absorption spectra for different illumination conditions match our expectations for a Fano resonance. They show the importance of a spectral measurement of the near-field energy storage to determine the spectral properties of the resonant channel.

We have theoretically analysed and experimentally demonstrated a Fano resonance in the scattering spectra of individual subwavelength semiconductor nanostructures such as a Si nanostripe. The changes in the Fano line shape that result for different illumination conditions and stripe sizes could be attributed to modifications in the far-field interference between resonant and background scattering processes. Configuring the same Si nanostripe into a photodetector also opened the unique opportunity to determine the spectral properties of the near-field energy storage occurring in the resonant scattering channel by a direct photocurrent/light absorption measurement. By means of the absorption measurement we were able to experimentally follow the flow of light through the resonant scattering channel in addition to the ultimate Fano interference in the far-field. The ability to simultaneously measure light absorption and scattering enhanced our fundamental understanding and practical use of Fano resonances. It may also enable new studies aimed at exploring the intriguing interplay between Fano resonances and the generation of optical vortices with nanostructures[30].

Methods

Device fabrication. The MSM photodetector was generated in a multistep process. First, a 50-nm-thick intrinsic poly-Si film was deposited onto a quartz substrate in a low-pressure chemical vapour deposition tool at 620 °C. Then, electron beam lithography and standard reactive-ion etching (HBr/Cl_2) were employed to define nanostripes of different widths. Finally, electron beam lithography, metal evaporation and lift-off were used to define electrical contacts to both ends of the fabricated nanostripes.

Optical characterization. The complex refractive index of the deposited poly-Si thin film was measured with a spectroscopic ellipsometer (Woollam). Scattering spectra from Si nanostripes were measured by illuminating the devices with a halogen lamp and collecting the scattered light confocally using a ×50 objective (Nikon). This light was sent to a spectrometer-coupled CCD (charge-coupled device; Princeton Instruments) for spectroscopy measurements.

Photocurrent measurements. The excitation beam in the photocurrent measurements was obtained from a supercontinuum laser coupled to an acousto-optical tunable filter (Fianium). A ×50 objective was used to focus the light onto the photodetector and the spatial distribution of the phototocurrent was measured by raster-scanning the illumination spot over the sample with an *XYZ* piezo-stage (Physik Instrumente NanoCube). To obtain high-signal-to-noise ratio photocurrent measurements, the illumination source was chopped and the photocurrent signal was measured using a source meter (Keithley) coupled to a lock-in amplifier (Stanford Research Systems).

Received 28 July 2013; accepted 27 February 2014; published online 20 April 2014

References

1. Fano, U. Effects of configuration interaction on intensities and phase shifts. *Phys. Rev.* **124,** 1866–1878 (1961).
2. Luk'yanchuk, B. *et al.* The Fano resonance in plasmonic nanostructures and metamaterials. *Nature Mater.* **9,** 707–715 (2010).
3. Fedotov, V. A., Rose, M., Prosvirnin, S. L., Papasimakis, N. & Zheludev, N. I. Sharp trapped-mode resonances in planar metamaterials with a broken structural symmetry. *Phys. Rev. Lett.* **99,** 147401 (2007).
4. Fan, S. & Joannopoulos, J. D. Analysis of guided resonances in photonic crystal slabs. *Phys. Rev. B* **65,** 235112 (2002).
5. Christ, A., Tikhodeev, S. G., Gippius, N. A., Kuhl, J. & Giessen, H. Waveguide-plasmon polaritons: Strong coupling of photonic and electronic resonances in a metallic photonic crystal slab. *Phys. Rev. Lett.* **91,** 183901 (2003).
6. Liu, N. *et al.* Plasmonic analogue of electromagnetically induced transparency at the Drude damping limit. *Nature Mater.* **8,** 758–762 (2009).
7. Chen, C. Y., Un, I. W., Tai, N. H. & Yen, T. J. Asymmetric coupling between subradiant and superradiant plasmonic resonances and its enhanced sensing performance. *Opt. Express* **17,** 15372–15380 (2009).
8. Lahiri, B., Khokhar, A. Z., De La Rue, R. M., McMeekin, S. G. & Johnson, N. P. Asymmetric split ring resonators for optical sensing of organic materials. *Opt. Express* **17,** 1107–1115 (2009).
9. Zheludev, N. I., Prosvirnin, S. L., Papasimakis, N. & Fedotov, V. A. Lasing spaser. *Nature Photon.* **2,** 351–354 (2008).
10. Chang, W-S. *et al.* A plasmonic Fano switch. *Nano Lett.* **12,** 4977–4982 (2012).
11. Samson, Z. L. *et al.* Metamaterial electro-optic switch of nanoscale thickness. *Appl. Phys. Lett.* **96,** 143105–143103 (2010).
12. Sonnefraud, Y. *et al.* Experimental realization of subradiant, superradiant, and Fano resonances in ring/disk plasmonic nanocavities. *ACS Nano* **4,** 1664–1670 (2010).
13. Fan, J. A. *et al.* Self-assembled plasmonic nanoparticle clusters. *Science* **328,** 1135–1138 (2010).
14. Verellen, N. *et al.* Fano resonances in individual coherent plasmonic nanocavities. *Nano Lett.* **9,** 1663–1667 (2009).
15. Prodan, E., Radloff, C., Halas, N. J. & Nordlander, P. A hybridization model for the plasmon response of complex nanostructures. *Science* **302,** 419–422 (2003).
16. Miroshnichenko, A. E., Flach, S. & Kivshar, Y. S. Fano resonances in nanoscale structures. *Rev. Mod. Phys.* **82,** 2257–2298 (2010).
17. Ye, Z. *et al.* Mapping the near-field dynamics in plasmon-induced transparency. *Phys. Rev. B* **86,** 155148 (2012).
18. Walsh, G. F. & Dal Negro, L. Enhanced second harmonic generation by photonic–plasmonic Fano-type coupling in nanoplasmonic arrays. *Nano Lett.* **13,** 3111–3117 (2013).
19. Bohren, C. F. & Huffman, D. R. *Absorption and Scattering of Light by Small Particles* (Wiley, 1983).
20. Cao, L. *et al.* Engineering light absorption in semiconductor nanowire devices. *Nature Mater.* **8,** 643–647 (2009).
21. Cao, L. Y., Fan, P. Y., Barnard, E. S., Brown, A. M. & Brongersma, M. L. Tuning the color of silicon nanostructures. *Nano Lett.* **10,** 2649–2654 (2010).
22. Muskens, O. L. *et al.* Large photonic strength of highly tunable resonant nanowire materials. *Nano Lett.* **9,** 930–934 (2009).
23. Cao, L. Y., Park, J. S., Fan, P. Y., Clemens, B. & Brongersma, M. L. Resonant germanium nanoantenna photodetectors. *Nano Lett.* **10,** 1229–1233 (2010).
24. Schuller, J. A., Taubner, T. & Brongersma, M. L. Optical antenna thermal emitters. *Nature Photon.* **3,** 658–661 (2009).
25. Cao, L. *et al.* Semiconductor nanowire optical antenna solar absorbers. *Nano Lett.* **10,** 439–445 (2010).
26. Fan, P. *et al.* An invisible metal-semiconductor photodetector. *Nature Photon.* **6,** 380–385 (2012).
27. Ruan, Z. & Fan, S. Temporal coupled-mode theory for Fano resonance in light scattering by a single obstacle. *J. Phys. Chem. C* **114,** 7324–7329 (2010).
28. Søndergaard, T. & Bozhevolnyi, S. Strip and gap plasmon polariton optical resonators. *Phys. Status. Solidi B* **245,** 9–19 (2008).
29. Fan, S., Suh, W. & Joannopoulos, J. D. Temporal coupled-mode theory for the Fano resonance in optical resonators. *J. Opt. Soc. Am. A* **20,** 569–572 (2003).
30. Luk'yanchuk, B. S., Miroshnichenko, A. E. & Yu, S. K. Fano resonances and topological optics: an interplay of far- and near-field interference phenomena. *J. Opt.* **15,** 073001 (2013).

Acknowledgements

We acknowledge financial support from the Global Climate and Energy Project at Stanford University and the Department of Energy Grant No. DE-FG07ER46426.

Author contributions

P.F., Z.Y., S.F. and M.L.B. conceived the ideas for this paper. P.F. and Z.Y. designed, fabricated and simulated the device structures. P.F. wrote the initial draft of the manuscript. S.F. and M.L.B. supervised the project.

Additional information

Supplementary information is available in the online version of the paper. Reprints and permissions information is available online at www.nature.com/reprints. Correspondence and requests for materials should be addressed to P.F. or M.L.B.

Competing financial interests

The authors declare no competing financial interests.